OUKA
The University of Osaka
Institutional Knowledge Archive

Title	Experimental evidence of ionization burnthrough and absorption resonance in radiative energy transport in hot dense matter
Author(s)	Mochizuki, T.; Mima, K.; Ikeda, N. et al.
Citation	Physical Review A. 1987, 36(7), p. 3279-3287
Version Type	VoR
URL	https://hdl.handle.net/11094/3264
rights	Mochizuki, T., Mima, K., Ikeda, N., Kodama, R., Shiraga, H., Tanaka, K.A., Yamanaka, C., Physical Review A, 36, 7, 3279-3287, 1987-10-01. "Copyright 1987 by the American Physical Society."
Note	

The University of Osaka Institutional Knowledge Archive : OUKA

https://ir.library.osaka-u.ac.jp/

The University of Osaka

Experimental evidence of ionization burnthrough and absorption resonance in radiative energy transport in hot dense matter

T. Mochizuki, K. Mima, N. Ikeda, R. Kodama, H. Shiraga, K. A. Tanaka, and C. Yamanaka
Institute of Laser Engineering, Osaka University, 2-6 Yamada-oka, Suita, Osaka 565, Japan
(Received 29 December 1986)

Radiative energy transport in hot dense matter has been investigated in the sub-keV region. In a medium-Z element (aluminum), ionization burn-through has been observed. Burn-through speed is estimated to be 6×10^5 g/cm^2 sec or more at an x-ray intensity of 7.4×10^{12} W/cm^2. At a high Z (gold), the spectral structure of transmitted x rays indicates the formation of an x-ray heat conduction band via absorption resonance. Penetration depth ($\rho\,\Delta R$) of radiative energy transport in Au is found to be 3–4 times larger than that in aluminum.

I. INTRODUCTION

Physics of radiative energy transport in high-density plasmas is one of the critical issues to clarify the equation of state of high–energy-density matter. Details of its physics have still remained unclear, such as high-density effect, ionization effect, etc. Few experimental results relevant to this subject have been obtained with use of laboratory-scale high-power glass lasers.[1–4] Among them, Mizui's result[2] suggested that the radiative heat conduction in a solid gold foil may penetrate long distance up to several micrometers with a constant intensity. In their experiment, however, precurser laser light such as an amplified spontaneous emission might have heated and ablated the foil before the main laser pulse arrived.[5]

McLean *et al.* found that when 1-μm laser heated the front surface of 4–12-μm-thick Al foils, x rays were a major energy carrier to heat the rear surface up to several electron volts.[6] Computational studies of the above experimental result were also reported.[7,8] Duston *et al.* claimed that the ionization front driven by the radiative preheat causes the reduction of the opacity, resulting in strong radiative energy transport to the rear side of the foil,[7] and they also pointed out that a cooperative work of radiation and thermal electrons dominated the hydrodynamics of a laser-heated plasma even if it is a low-Z element such as carbon.[9]

At high Z, the energy transport towards the overdense region from the laser-heated region was mostly carried out by sub-keV x rays,[10,11] driving a thermal radiative heat wave into the solid density.[10] X-ray confinement in a hollow Au cavity heated by a laser will be strongly coupled with the radiative energy diffusion into the cavity wall.[12,13] However, no direct observation has been made of the transport dynamics of soft x rays which play a critical role in hot dense matter.

In this paper we report the first experimental investigation of sub-keV radiative energy transport in hot dense matters using a double-foil technique, by which it is possible to heat a rear foil only by x rays. The experimental results show the evidence of the ionization burn through predicted by Duston for aluminum foil and indicate the formation of heat conduction bands in x-ray frequency domain for gold foil.

II. EXPERIMENTAL CONDITION

The experiments have been carried out at the schematic shown in Fig. 1. The first layered foil consisting of typically 500-Å-thick gold and 0.2-μm parylene (CH) layers is heated by a 0.53-μm Gaussian laser pulse through an aspheric lens of $f/1.6$ at an intensity of 2.0×10^{14} W/cm^2 in an effective spot diameter of 220 μm in a 350±30 psec full width at half maximum with an incidence angle of 54°. Details of laser intensity distribution are described in Ref. 10.

Either Al or Au foil is used for the second foil. Intense soft x rays emitted from the rear side of the first foil irradiates the second foil. Time-integrated soft x-ray spectral intensities towards the front and rear sides of the first foil were measured by a set of ten channel-filtered biplanar x-ray diodes (XRD) which had aluminum photocathodes.[10] The laser spot was monitored by 45-μm-thick Be-filtered x-ray pinhole cameras at both sides.

The vacuum gap distance between the first and second

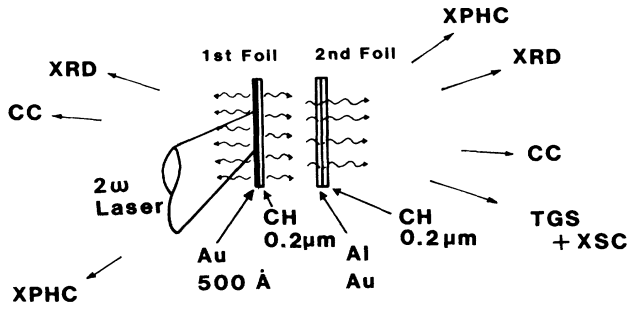

FIG. 1. A schematic view of the experimental setup. Laser: 0.53 μm wavelength Gaussian pulse with an intensity of 2×10^{14} W/cm^2 in 350 psec. XRD: A set of ten channel-filtered x-ray diodes. XPHC: X-ray pinhole camera; CC, charge collector; TGS, transmission grating spectrometer; XSC, soft-x-ray streak camera. The first foil is used as an x-ray emitter. CH is a parylene layer.

 ©1987 The American Physical Society

foils was fixed at 150 μm. This distance is long enough to minimize the effect to the second foil of the hydrodynamic shock wave and heated thermal electrons produced at the place where the laser deposits its energy. All the foils used were supported by a 0.2-μm parylene layer, except for a 0.3-μm Al foil which was free standing, and mounted on 390-μm-thick brass washers whose inner and outer diameters were 2.1 and 4.2 mm, respectively. The second foil was electrically insulated.

A transmission grating spectrometer coupled with a soft-x-ray streak camera was mounted at the rear side of the foils to measure time-resolved spectra in the range of 100 eV to 1 keV with a spectral resolution of 4 Å. The time scale of the streak camera was calibrated by a double laser pulse technique. The time resolution was estimated to be typically about 30 psec. The overall spectral response was indirectly estimated by comparing with a time-integrated spectrum obtained from the XRD signals. Charge collectors were mounted at both front and rear sides near the target normal to monitor the ion time-of-flight spectrum.

III. RESULTS AND DISCUSSIONS

First we measured the rear emission from the first foil by the XRD as a function of gold-layer thickness without mounting the second foil. The signal of parylene-filtered XRD which corresponds to 150–280-eV x rays increased with Au-layer thickness up to 500 Å and decreased at 1000 Å by about 10% of the value at 500 Å. The optimum thickness of 500 Å is in reasonable agreement with the mass ablation depth which is estimated by the experimental result[3] at several micrometers thick Au foils.

Figure 2 shows time-integrated spectral intensities of the front and rear emissions which were obtained by the ten-channel XRD for a 500-Å-thick Au layer. It should

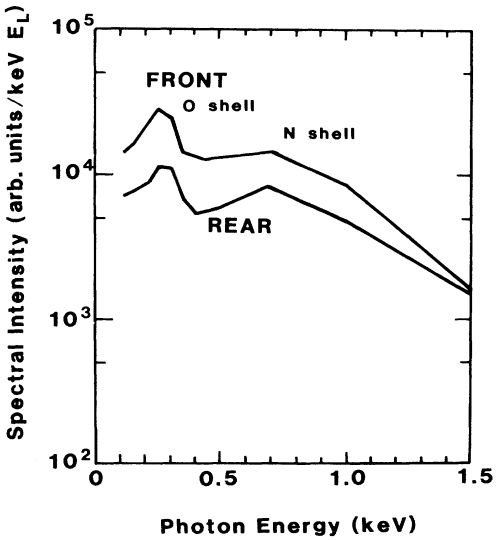

FIG. 2. Time-integrated spectral intensities of the front and rear emissions from a 500-Å-thick Au foil. Laser parameters are described in Fig. 1. E_L is the laser energy.

be noted that the rear emission spectrum has a more prominent structure due to *O*-shell and *N*-shell emissions, a deeper valley about 400 eV, than the front emission, while the front emission has a spectral shape similar to that from an Au block target.[10] In order to evaluate the effect on the observed rear emission spectrum by the 0.2-μm-thick parylene (CH) substrate, another 0.2-μm-thick CH foil was placed as the second foil, but the observed spectrum was identical within $\pm 10\%$ to that obtained without the second CH foil. The x-ray conversion efficiency in 0.1 to 1.5 keV which is defined as the ratio of a time-integrated x-ray flux to the incident laser energy was 25% towards the front and 15% towards the rear; a total of conversion efficiency was 40%. Typical x-ray signal in the streak camera shows that the radiation is emitted towards the rear in a 320 psec full width at half maximum for 200 eV and a little shorter for 1000 eV as shown in Fig. 3(a).

From the above results, the intensity of the rear emission (we call it primary x ray hereafter) is determined to be 7.4×10^{12} W/cm^2 at the second foil taking into account a geometrical reducing factor ~ 0.35 which originates in a finite size of the x-ray emitter and a distance of the two foils, and also taking into account a spatial distribution of the primary x-ray intensity at the second foil. We averaged over the primary x-ray intensity in the spot area on the second foil whose diameter is the same as the laser spot on the first foil. The average intensity is 0.7 $I_{x,0}$ where $I_{x,0}$ is the intensity at the center of the spot area. We could not measure directly the intensity distribution at the second foil. When the x-ray transmission through the second foil was measured, we always used 500-Å-thick Au foils as the x-ray emitter.

The charge collector signals showed very smooth velocity distributions to the rear and front directions, both of which had a peak at about 3×10^7 cm/sec. The front signal had an additional precurser peak which is inferred to be due to fast protons. The observed ion velocity to the rear direction corresponds to an electron temperature of about 500 eV assuming an isothermal expansion of the foil. Hydrodynamic code calculation shows that the electron density is maintained during the laser heating at a significantly higher level than the density of the laser turning point due to slow hydrodynamic expansion of heavy Au ions, indicating that the transmission of the laser light is negligible for the 500 Å Au on 0.2 μm CH foil. This conclusion is also supported indirectly in an x-ray pinhole image through the second foil; the keV x-ray pinhole image would otherwise contain a much larger hot area heated by the leaked laser light in the second foil than that in the first foil.

Other energy fluxes into the second foil may be divided into the following several components: (i) plasma ion particles, (ii) hot electrons, and (iii) radiation from the plasma trapped between the two foils. The intensity of the plasma ions is estimated to be less than 8×10^8 W/cm^2 from the charge collector signal. Their arrival to the second foil was confirmed to be only after the laser pulse in this experiment. Heat flux by the hot electrons, (ii), which is generated at the laser-heated region is estimated to be less than 10^{-3} of that by cold elec-

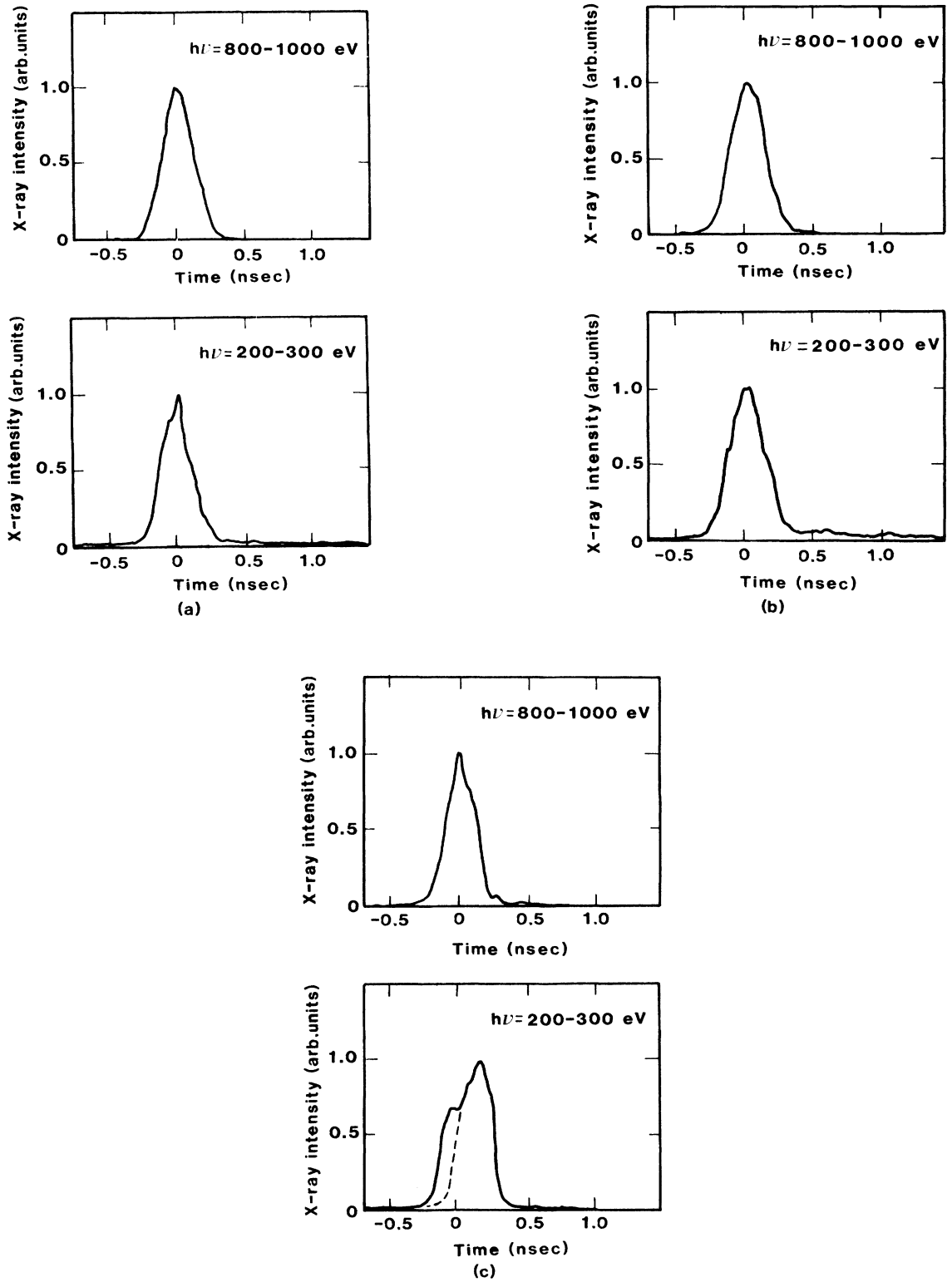

FIG. 3. Temporal behaviors of (a) x-ray pulse emitted towards the rear of the 1st foil, (b) x ray transmitted through the second foil consisting of 0.1-μm-thick Al and 0.2 μm parylene layers, and (c) x ray transmitted through the 0.3-μm-thick Al second foil. The intensities are normalized by the peak.

trons.[10] In addition the flux reaching the second foil would be much less since vacuum insulation is effective for stopping the hot electrons.[14] Hence these two components are four or more orders of magnitude less than the radiative energy flux. The x-ray emission from the stagnated plasma was observed only 0.5 nsec after the laser heating pulse, but the intensity was negligible. Therefore only radiative energy flux from the laser-heated foil is a major heating flux to the second foil during the laser heating phase.

Figure 3(b) shows an x ray transmitted through the second foil consisting of 0.1-μm-thick Al and 0.2 μm CH layers. Figure 3(c) shows an x ray for the 0.3-μm-thick Al foil. It is found that all the transmitted x rays have a pulse shape similar to that of the incident primary x rays except for lower-energy photons (200–300 eV) which show a long-lived low-level emission for the 0.1 μm Al and a delayed peak for the 0.3 μm Al. The positions of the time origins for Figs. 3(a)–3(c) are not identical because of the trigger jitter in the streak camera. However, the signal peak of transmitted high-energy x rays, say 800–1000 eV photons should correspond to the maximum intensity of the primary x rays, i.e., the laser intensity peak, because these x rays easily shinethrough the second foil. So we can use the time of the appearance of these signal peaks as the time reference in each shot. The long-lived emission is inferred to be due to the afterglow during radiative cooling phase after the x-ray heating and/or due to the emission from the stagnated plasma. Therefore we concentrate on the x ray transmitted at the heating phase and evaluate the amount of spectrally resolved transmitted, i.e., rear emitted, radiation by integrating the intensity in the time period of the x-ray heating pulse.

Figure 4 shows the spectrally resolved x-ray intensities which were obtained as described above as a function of Al thickness. Dashed lines correspond to the x-ray attenuation due to photoionization absorption[15] in a cold Al. The x-ray intensity is normalized to that obtained with no Al layer. The emissivity of the 0.2 μm CH layer is two orders of magnitude lower than that of Au,[10] so its fluorescence is negligible in the observed radiation. It is clearly seen that the transmission of 100–300 eV photons gradually decreases as the Al layer thickness increases, but its level is significantly higher than the transmission for a cold Al up to 0.3 μm thickness. The observed transmission rate η_{tr} of 100–300 eV photons decreases with the foil thickness d_0 linearly as

$$\eta_{tr}=1-0.28\left[\frac{d_0}{0.1\ \mu\text{m}}\right] \tag{1}$$

rather than exponentially. On the other hand the attenuation of the intensities of 500–1000 eV photons approximately follows the dashed lines. If three-dimensional (3D) expansion dominated the hydrodynamic motion of the radiatively heated foil, it would cause the opacity reduction in the whole photon energy range, resulting in the enhanced transmission also in the higher-energy range. The observed anomalous transmission at 100–300 eV in the time of concern suggests that the 3D expansion of the heated foil is not the case. The change of transmission behavior at 500 to 200 eV is considered to be due to the drastic change of opacity in lower- and higher-energy sides of the L absorption edge (100–400 eV) of aluminum ions, especially when their charge states are $+5$ to $+8$.

The above result is best explained by the ionization burn-through process predicted by Duston *et al.*;[7] absorbed radiation is collisionally quenched, resulting in increased temperature and ionization of the Al layer, while the temperature rise shifts the L absorption edge $\sim$100 eV to the higher energy $\sim$300 eV, i.e., the blue shift of the edge occurs, as shown in Fig. 2 of Ref. 7, so the opacity decreases behind the ionization front. Finally shine-through radiation comes out from the rear side of the foil with an enhanced transmission of 100–300 eV x rays as shown in Fig. 4. This indicates that most of the aluminum ions were ionized up to the charge state of $+7$ whose L absorption edge was about 300 eV. Local thermodynamic equilibrium (LTE) calculation shows that Al^{+7} is mostly populated at the electron temperature of about 100 eV at solid density. So it is likely that the present primary x-ray flux heated the Al foil up to about 100 eV.

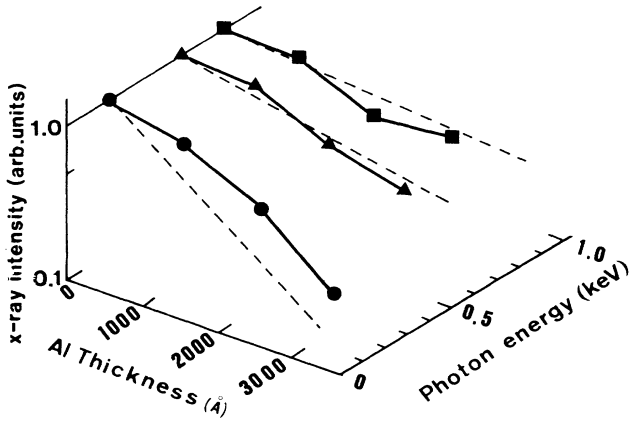

FIG. 4. Spectrally resolved intensities of the x rays transmitted through the Al second foil as a function of Al thickness. The intensity normalized to that obtained with no Al layer. Dashed lines correspond to the x-ray attenuation due to the photoionization absorption in a cold Al.[15]

In the dense plasmas discussed above, the energy levels are displaced by Debye screening of the ion potential, resulting in a continuum lowering. A red shift of the edge $\Delta I\sim -3Z^*e^2/2R_i$ (Ref. 16) is estimated to be -90 and -40 eV for the ion density 5×10^{21} cm^{-3}, respectively, assuming $Z^*\sim7$ at $T_e=T_i=100$ eV, where Z^* is the average charge of ions and R_i is an ion-sphere radius defined by the relationship $4\pi R_i{}^3N_e/3=Z^*$. Thus the red shift described above compensates the blue shift ($\sim$300 eV) only in a so small fraction that the ionization burn-through process is maintained to be effective in the present experiment.

The rear surface may be preheated instantaneously by shine-through high-energy photons of 500 eV–1 keV and then may re-emit lower-energy photons via frequency down-conversion process.[7] Their contribution to the

observed flux of low-energy x ray would be only in a negligible fraction except for the 0.3 μm Al foil because the absorbed energy of 500 eV–1 keV photons in the foil is one or two orders of magnitude smaller than that of 100–400 eV photons. For 0.3 μm Al foil it is found that the signal level of low-energy photons is about one fifth of that without the Al foil. Thus the signal level of the reemitted low-energy photons described above may be comparable in this case to that of the low-energy photons which shined through after the ionization burn-through front reached the rear side.

We did not see significant difference in time of appearance and temporal shapes of x-ray pulses at 100–300 eV and 700–1000 eV for the foil thickness up to 0.2 μm. This fact may be partly due to the finite time resolution of the streak camera, but more intrinsically would be due to a two-dimensional distribution of the primary x-ray intensity on the foil surface which blurs the arrival time of ionizing front, and/or due to a diffused structure of the ionizing front.

However, it is found that low-energy photons (200–300 eV) for 0.3 μm foil appear in the streak camera with a pulse shape which is composed of two parts as shown in Fig. 3(c). One is a smaller hump at earlier time and the other the signal peak at later time. The two-dimensional distribution of the primary x-ray intensity at the second foil is a smooth function that gradually decreases towards the peripheral part of the heated area. Therefore it is unlikely that the two-dimensional distribution caused the stepwise variation in the spatially integrated x-ray streak signal as shown in Fig. 3(c). The first hump corresponds to the appearance of high-energy photons (800–1000 eV), thus seems to be due to the instantaneous heating by the high-energy photons as discussed previously. The second peak tends to delay by about 100 psec compared to the 800–1000 eV photons and is inferred to have a rising part as shown by a dashed line in Fig. 3(c). This indicates that the delayed appearance of low-energy photons is caused by the time period of traveling of the ionization burn-through front.

The ionization burn-through depth defined as the foil thickness at $1/e$ transmitted x-ray intensity is determined from Fig. 4 to be about 6×10^{-5} g/cm^2. The nominal average velocity of the ionization front is thus estimated to be about 6×10^5 g/cm^2 sec by dividing the depth by the time delay.

The ionization burn-through speed $V_{\rm IB}=\rho\,dx/dt$ is evaluated by the equation of energy conservation,

$$\rho E_z\,dx = I_x\eta_{\rm ab}\,dt - \dot{E}_{\rm exp}(t)dt\ , \tag{2}$$

assuming that the opacity is reduced to a negligible level after the absorption edge is blue shifted via x-ray heating, i.e., the plasma becomes transparent to the incident x ray coming thereafter. E_z is the energy loss per unit mass consisting of the ionization energy loss and the thermal energy of plasma,

$$E_z = M^{-1}\left[\sum_{i=0}^{z^*} I_i + \tfrac{3}{2}(Z^*+1)k_B T_e\right]\ , \tag{3}$$

where I_i is the ionization energy of the ith multiple ion and Z^* is the average ion charge which is achieved at a LTE state of plasma. M is the ion mass. $\dot{E}_{\rm exp}$ is the cooling rate by the hydrodynamic expansion of the plasma. I_x, $\eta_{\rm ab}$, and $\rho\,dx$ are the incident x-ray intensity, the effective absorption in the foil of the spectrally integrated primary x rays, and the areal mass density, respectively.

Here as the most probable value to explain the result in Fig. 4, we adopt $T_e\sim100$ eV at which an Al atom is ionized up to Al^{+7} in the LTE condition and thus the blue shift of the edge to 300 eV occurs. We neglect $\dot{E}_{\rm exp}$ at the first step. From Fig. 2 and the absorption cross section, $\eta_{\rm abs}$ is estimated to be about 0.35 for the photon energy range of interest. Then the average ionization burn-through speed $V_{\rm IB}$ is found to be 4×10^5 g/cm^2 sec; 1.5×10^5 cm/sec for a solid density Al, at the x-ray absorbed intensity $I_x\eta_{\rm ab}$ of 2.6×10^{12} W/cm^2. This value is in reasonable agreement with the experimental result if we take into account that our model is not a completely self-consistent one. For example, we neglect the effect of hard x ray (500–1000 eV) preheating.

After the ionization burn-through crosses the Al foil, the hydrodynamic expansion becomes a dominant cooling mechanism. When the absorption edges shift to below 300 eV due to the expansion cooling, the soft x rays are absorbed efficiently to heat up the plasma. As the result the average ionization state Z^* is kept constant, 7. During the x-ray pulse, the Al plasma expands to the thickness of $d\simeq C_s\tau_x$. When $Z^*=7$ is required, the LTE ionization relation gives

$$k_B T_e \simeq 100(n/n_{\rm solid})^{0.2}\ {\rm eV}\ , \tag{4}$$

according to the average ion model[17] where n is the ion number density. Since $n/n_{\rm solid}=d_0/d$ we obtain $k_B T_e=39$ and 48 eV at $d_0=0.1$ and 0.3 μm, respectively, and $n\approx6\times10^{20}(d_0/0.1\ \mu{\rm m}){\rm cm}^{-3}$. When Z^* is assumed to be constant during the expansion, the temperature depends weakly on the density as shown by Eq. (6). Therefore the cooling rate $\dot{E}_{\rm exp}$ is approximately evaluated by using a self-similar solution of one-dimensional isothermal expansion of the foil which is uniformly heated by the x-ray pulse. From the self-similar analysis we obtain the expansion energy $\dot{E}_{\rm exp}$ as

$$E_{\rm exp}=\dot{R}^2\rho_0 d_0/2=\rho_0 d_0 C_s^2\ln(R/R_0)\ , \tag{5}$$

(see Appendix) where ρ_0 and d_0 are the initial mass density and foil thickness, respectively, and the initial density profile is assumed to be $\rho_0\exp(-x^2/2R_0^2)$ and $R_0=d_0/\sqrt{2\pi}$. C_s is the sound speed in the x-ray heated plasma and $R(t)$ is determined by Eq. (A10) in the Appendix.

By integrating the energy balance equation over the x-ray heating time τ_x, we obtain the energy necessary for ionization burn through and keeping the average ionization state constant during expansion as follows:

$$E_{\rm tot}=\rho_0 d_0 E_z + E_{\rm exp} \tag{6}$$

[see Appendix, Eq. (A13)]. Note that E_z is the value for the expanding rarefied plasma. Thus $E_{\rm tot}$ of the expanding plasma is evaluated to be

$$E_{\text{tot}} = 248 \left[\frac{d_0}{0.1\ \mu\text{ m}} \right] \text{J/cm}^2 \ . \tag{7}$$

On the other hand, the total plasma energy at $k_B T_e = 11$ eV and the solid density where $Z^* \sim +7$ was

$$E_{\text{tot}} = \rho_0 d_0 E_z = 187 \left[\frac{d_0}{0.1\ \mu\text{m}} \right] \text{J/cm}^2 \ . \tag{8}$$

The energy required to keep Z^* in the expanding plasma constant is about $61[d_0/(0.1\ \mu\text{m})]$ J/cm^2. Namely, about $\frac{1}{4}$ of the total plasma energy of the expanding plasma is considered to be absorbed after the ionization burnthrough. Note that the total plasma energy is proportional to d_0 when Z^* is kept constant and the transmission rate of the x rays, η_{tr}, is given by

$$\eta_{\text{tr}} \simeq \frac{E_{x,0} - 248 d_0/(0.1\ \mu\text{m})}{E_{x,0}} = 1 - 0.30 \left[\frac{d_0}{0.1\ \mu\text{m}} \right] , \tag{9}$$

which reasonably agrees with the experimental data represented by Eq. (1), where $E_{x,0} = 822$ J/cm^2 is the primary x-ray flux.

Somewhat better agreement may be obtained if the fluorescence intensity is taken into account in the above analysis. The experimental results in Fig. 4 include some fluorescences by direct-frequency down conversion of high-energy photons as suggested in Fig. 3(c).

We believe that the above analysis suffices to prove that the obtained results have been caused by the ionization burn-through process, although a more accurate quantitative explanation could be provided by hydrodynamical computer simulations which incorporate a precise radiation line transport calculation as well as atomic rate equations.

Similar experiments have been made using the Au second foil. Figure 5 shows the results obtained in the same way as for Fig. 4. Lowest-energy channel had a more prominent fluorescence signal level as shown in Fig. 6 after the heating laser pulse than that for Al, whereas higher-energy photons produced a pulse shape similar to the incident x rays shown in Fig. 3(a). It should be noticed that 150–250 and 600–700 eV photons are emitted more strongly than 350–450 and 900–1000 eV photons which are monotonically attenuated according to the photoabsorption (dashed lines) for a cold Au with the Au thickness. The transmitted radiations are enhanced not only by the shine through which has been discussed previously, but also by the reemission from the x-ray heated second foil because a significant fraction of high-energy x rays is absorbed in such high-Z matter. The second process is seen as equivalent to the effective energy transmission through the Au layer. The enhanced energy transports at 150–250 and 600–700 eV channels correspond to the electronic transitions in O shell and N shell of gold ions, respectively, as seen in the emission spectrum at a laser-heated Au plasma.[10] We consider a possibility that the energy levels in these orbital shells are so dense that the strong reemission process forms the effective heat conduction band in x-ray frequency domain via "absorption resonance." This has similarity to the electron conduction band in semiconductor. The existence of absorption resonance has been only indirectly suggested by the anomalous optical constants of Au derived from the diffraction measurements of an Au transmission grating.[18] The frequency of the photons incident to the

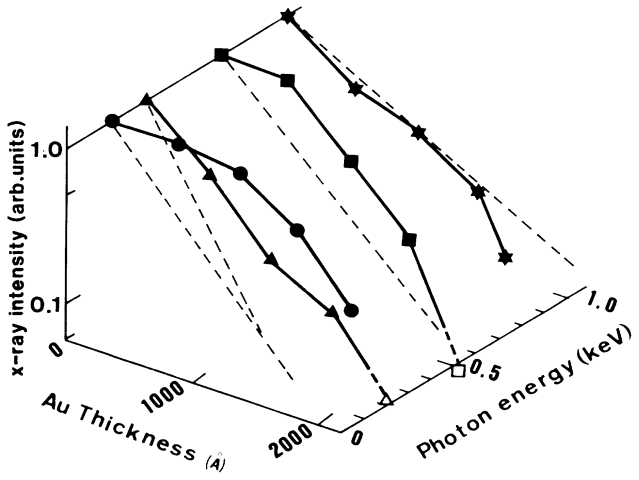

FIG. 5. Spectrally resolved intensities of the x rays transported in the Au second foil as a function of Au thickness. The intensity is normalized to that obtained with no Au layer. Dashed lines correspond to the x-ray attenuation in a cold Au.[15]

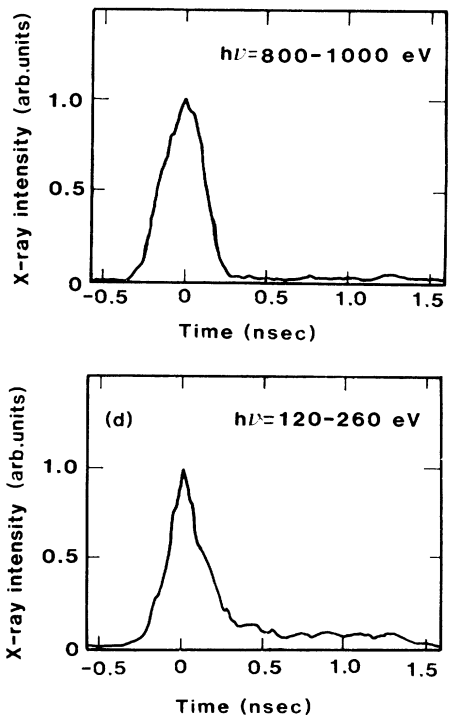

FIG. 6. X ray transported in the second foil consisting of 0.1-μm-thick Au and 0.2-μm CH layers. The intensities are normalized by the peak.

second foil would be strongly down converted during energy penetration. Thus the energy transport should be concentrated on the conduction bands described above. However, the radiative cooling and the ionization energy loss limit the radiative energy-transport depth in the Au foil. In the present case, an effective x-ray mass penetration depth (g/cm^2) is found to be 3–4 times larger than that in Al layer. The physical picture described above may be still premature. Further study is needed to obtain more detailed understandings on physics and quantitative explanation of radiation transport in high-Z matter.

The obtained results and the above discussions suggest to us that low-Z and medium-Z elements will easily become transparent to intense soft x rays by the ionization burn-through process, and also suggest to us that even in a high-Z element strong radiative energy transport may take place through the process which is similar to the self-induced transparency process[19] in the laser interaction with nonlinear optical medium. Both processes operate to heat the inner part of the matter so efficiently that they may produce some difficulty in laser fusion scheme; the preheating of the fuel pellet may easily occur with intense soft x rays.

Particularly, if the incident radiation intensity increases beyond the limited value $I_{x,\text{limit}}$, then the hydrodynamic deflagration wave can never catch up with the radiation-driven ionization front. Using Eq. (2) and $V_{IB}(I_{x,\text{limit}}) \gtrsim C_s$, we obtain

$$I_{x,\text{limit}} = 9\frac{n_0^{16/7}}{A^{8/7}} \times 10^{14} \text{ W/cm}^2 , \tag{10}$$

where n_0 is the density in 5×10^{22} cm^{-3} and A is the atomic mass number. Hence we assumed a blackbody radiation with a radiation temperature T_R, as the incident x ray and $T_e \sim T_R$, and E_z is given as $2Zk_BT_e/M$ by the approximate estimation of $\sum I_i \sim ZI_z/2 \sim Zk_BT_e/2$. For example, $I_{x,\text{limit}} = 2\times10^{13}$ and 5×10^{13} W/cm^2 for $A = 27$ (Al) and 12 (C) at $n_0 \simeq 1$ (solid density), respectively.

More accurately, the absorption by free-free transitions and weak bound-free transitions behind the ionization front will attenuate x-ray flux sustaining the ionization front so that $I_{x,\text{limit}}$ should be higher than that given by Eq. (10). However, since hydrodynamic expansion reduces the free-free opacity a heated layer is formed by ionization burn through in front of the rarefraction wave as a precurser.

If the above physical process dominates the radiation-plasma interaction, then the first option of radiation drive in laser fusion scheme would be a "radiation-heated explosive acceleration" (RADEXA) in which some fractions of the outer part of a target shell are instantaneously heated by incident strong x radiation and then explosively expand to accelerate the remaining part of the shell. In this case the problem would be that the acceleration pressure decreases rather than increases as the compression proceeds.[20]

The second option of the pusher acceleration by x radiation is a radiation-drive ablative acceleration.[21] For this, high-Z doped low-Z ablator may be useful. Here high-Z material will stop x rays while low Z increases the sound speed achieving ablative acceleration. The red shift of the absorption edge by high-density effect[16] may become useful to suppress the ionization burnthrough if a high-density compressed region is substantiated initially by using laser direct-drive compression.

The third option may be such an acceleration that the incident x ray is efficiently transported through a high-Z tamper layer via resonance absorption as shown in Fig. 5 and strongly absorbed at a low-Z pusher, producing a strong plasma pressure therein. Then the inner low-Z pusher is accelerated inwards while the outer high-Z layer stays as a tamper.

We had experimental evidences for the third option early in 1982.[22,23] We obtained an x-ray backlighted image of a 0.1 μm Au-coated glass microballoon target which was irradiated by intense soft x rays from external sources. The picture showed clearly a double structure. The inner glass microballoon was accelerated inwards, while the Au layer was accelerated outwards as if it were peeled off from the glass microballoon surface. The above result indicates that the significant fraction of the incident soft-x-ray energy is transported through the Au layer to the interface between the Au and SiO_2 layers, heating this region and then the heated region expands to accelerate the SiO_2 and Au layers in opposite directions.

As far as the laser fusion is concerned, we need a further detailed investigation to assess the total energy efficiency of pellet compression by x radiation.

IV. CONCLUSION

Radiative energy transport has been investigated using double-foil targets in the sub-keV region for the first time. This target separates the energy transport by laser-heated bulk thermal electrons from radiative energy transport. In a medium-Z (Al) matter, ionization burn through has been clearly observed. Burn-through speed in Al is estimated to be 6×10^5 $\text{g/cm}^2\,\text{sec}$ at the x-ray intensity of 7.4×10^{12} W/cm^2. In a high-Z (Au) matter with strong reemission and reabsorption, radiative energy has been transported for a long distance (mass penetration depth 3–4 times larger than the case of Al). The spectral structure of rear emission indicates the formation of x-ray heat conduction band via absorption resonance.

The question still remains on whether the mass ablation front can catch up with the ionizing front at higher x-ray intensity, i.e., $\sim10^{14}$ W/cm^2. This would be strongly dependent on x-ray spectrum and absorption processes of matter.

ACKNOWLEDGMENTS

The authors greatly acknowledge invaluable comments by Dr. J. Davis of U.S. Naval Research Laboratory, U.S.A.

APPENDIX

The isothermal expansion of a thin foil which is uniformly heated is described by a self-similar solution.

The one-dimensional fluid equations are

$$\frac{\partial \rho}{\partial t}+\frac{\partial}{\partial x}(\rho V)=0 , \tag{A1}$$

$$\frac{\partial V}{\partial t}+V\frac{\partial}{\partial x}V=-\frac{1}{\rho}\frac{\partial P}{\partial x} , \tag{A2}$$

where ρ, V, and P are mass density, velocity, and pressure, respectively. When the temperature is constant, $P=\rho C_s^2$ for a constant sound velocity C_s. For the self-similar variable, $\xi=x/R(t)$, we set

$$\rho=\tilde{\rho}(\xi)/R(t) \quad \text{and} \quad V=\dot{R}(t)\tilde{V}(\xi) . \tag{A3}$$

Note that the total mass conservation $\int_{-\infty}^{\infty}\rho(x,t)dx=\rho_0 d_0$ is satisfied, where ρ_0 and d_0 are the initial density and the thickness, respectively.

Substituting (A3) into (A1), we obtain

$$-\tilde{\rho}-\xi\frac{d\tilde{\rho}}{d\xi}+\frac{d}{d\xi}(\tilde{\rho}\tilde{V})=0 , \tag{A4}$$

and

$$\ddot{R}\tilde{V}+\frac{\dot{R}^2}{R}-\xi\frac{d\tilde{V}}{d\xi}+\tilde{V}\frac{d\tilde{V}}{d\xi}=-\frac{C_s^2}{R\tilde{\rho}}\frac{d\tilde{\rho}}{d\xi} . \tag{A5}$$

Equation (A4) is integrated to obtain

$$\tilde{\rho}(\tilde{V}-\xi)=\text{const} . \tag{A6}$$

When $\tilde{V}$ is assumed to be zero at $\xi=0$, the constant of (A6) is zero. Therefore

$$\tilde{V}=\xi . \tag{A7}$$

Equations (A6) and (A7) yield

$$\frac{\ddot{R}R}{C_s^2}=-\frac{1}{\tilde{\rho}\xi}\frac{d\tilde{\rho}}{d\xi}=\beta \ (\text{constant}) . \tag{A8}$$

By replacing $R/\sqrt{\beta}$ and ξ/β by new R and ξ, the constant β is chosen to be unity.

Finally we obtain the following solutions,

$$\rho(x,t)=\frac{\tilde{\rho}_0}{R(t)}\exp\left[-\frac{\xi^2}{2}\right] \tag{A9}$$

and

$$\dot{R}^2=2C_s^2\ln(R/R_0) , \tag{A10}$$

where $\tilde{\rho}_0/R_0=\rho_0$ is the initial peak density and R_0 is related to the initial foil thickness, d_0 by the equation

$$\sqrt{2\pi}\tilde{\rho}_0=\rho_0 d_0 , \tag{A11}$$

namely, $R_0=d_0/\sqrt{2\pi}$.

The total expanding plasma energy, E_{tot}, is evaluated by

$$E_{\text{tot}}=\int_{-\infty}^{\infty}dx\left[\tfrac{1}{2}\rho V^2+\frac{1}{\gamma-1}\rho C_s^2\right]+\frac{\rho_0 d_0}{M}\sum_{i=0}^{z}I_i , \tag{A12}$$

where γ is the adiabatic constant. M is the ion mass, I_i is the ionization energy of the ith multiple ion and Z is the average ion charge which is achieved at a LTE state of plasma. Substituting (A9) with (A11) into (A12), we obtain

$$\begin{aligned}E_{\text{tot}}&=\frac{\rho_0 d_0}{M}\sum_{i=0}^{z}I_i+\frac{\rho_0 d_0}{2}\dot{R}^2+\frac{\rho_0 d_0 C_s^2}{\gamma-1}\\&\simeq\left[\rho_0 d_0\frac{\sum_{i=0}^{z}I_i}{M}+C_s^2\ln(R/R_0)+\frac{C_s^2}{\gamma-1}\right]\\&=[\rho_0 d_0 E_z+C_s^2\ln(R/R_0)] .\end{aligned} \tag{A13}$$

[1]T. Mizui, N. Yamaguchi, T. Yamanaka, and C. Yamanaka, Phys. Rev. Lett. **39**, 619 (1977).

[2]T. Mizui, N. Yamaguchi, S. Takagi, and K. Nishihara, Phys. Rev. Lett. **47**, 1000 (1981).

[3]H. Nishimura, F. Matsuoka, M. Yagi, K. Yamada, S. Nakai, G. H. McGall, and C. Yamanaka, Phys. Fluids **26**, 1688 (1983).

[4]A. Ng, D. Parfeniuk, L. DaSilva, and D. Pasini, Phys. Fluids **28**, 2915 (1985).

[5]H. Nishimura, K. Yamada, M. Yagi, F. Matsuoka, K. Nishihara, T. Yamanaka, and C. Yamanaka, Jpn. J. Appl. Phys. **22**, L786 (1983).

[6]E. A. McLean, S. H. Gold, J. A. Stamper, R. R. Whitlock, H. R. Griem, S. P. Obenschain, B. H. Ripin, S. E. Bodner, M. J. Herbst, S. J. Gitomer, and M. K. Matzen, Phys. Rev. Lett. **45**, 1246 (1980).

[7]D. Duston, R. W. Clark, J. Davis, and J. P. Apruzese, Phys. Rev. A **27**, 1441 (1983).

[8]D. Salzman, H. Szichman, and A. D. Krumbein, Phys. Fluids **30**, 515 (1987).

[9]D. Duston, R. W. Clark, and J. Davis, Phys. Rev. A **31**, 3220 (1985).

[10]T. Mochizuki, T. Yabe, K. Kodama, M. Hamada, N. Ikeda, S. Kiyokawa, and C. Yamanaka, Phys. Rev. A **33**, 525 (1986).

[11]R. Kodama, K. Okada, N. Ikeda, M. Mineo, K. A. Tanaka, T. Mochizuki, and C. Yamanaka, J. Appl. Phys. **59**, 3050 (1986).

[12]K. Okada, T. Mochizuki, N. Ikeda, M. Hamada, M. Mineo, R. Kodama, and C. Yamanaka, J. Appl. Phys. **59**, 2332 (1986); R. Pakula and R. Sigel, Z. Naturforsch. Teil A **41**, 462 (1986); G. D. Tsakiris *et al.*, Europhys. Lett. **2**, 213 (1986).

[13]T. Mochizuki *et al.*, in *Proceedings of the Eleventh International Conference on Plasma Physics and Controlled Nuclear Fusion Research, Kyoto, 1986* (IAEA, Trieste, 1986).

[14]H. Shiraga, S. Sakabe, K. Okada, T. Mochizuki, and C. Yamanaka, Jpn. J. Appl. Phys. **22**, L383 (1983).

[15]B. L. Henke, P. Lee, T. J. Tanaka, R. L. Shimabukuro, and B. K. Fujikawa, At. Data Nucl. Data Tables **27**, 1 (1982).

[16]J. Stewart and K. Pyatt, Astrophys. J. **144**, 1203 (1963).

[17]M. Itoh and T. Yabe, Phys. Rev. A **35**, 233 (1987); M. Itoh,

Master thesis, Osaka University, 1987 (unpublished).
[18]R. Tatchyn, I. Lindau, E. Källne, and E. Spiller, Phys. Rev. Lett. **53**, 1264 (1984).
[19]S. L. McCall and E. L. Hahn, Phys. Rev. Lett. **18**, 908 (1967); Phys. Rev. A **2**, 861 (1970).
[20]S. Bodner, J. Fusion Energy **1**, 221 (1981).
[21]T. Mochizuki *et al.* demonstrated this option experimentally; T. Mochizuki, S. Sakabe, K. Okada, H. Shiraga, T. Yabe, and C. Yamanaka, Jpn. J. Appl. Phys. **22**, L133 (1983).
[22]T. Mochizuki, Institute of Laser Engineering, Osaka University, 1984 (unpublished), Vol. 9, p. 17.
[23]T. Mochizuki, T. Yabe, K. Okada, and C. Yamanaka, *Laser Techniques in the Extreme Ultraviolet,* Proceedings of the Second Topical Meeting on Laser Techniques in the Extreme Ultraviolet, AIP Conf. Proc. No. 119, edited by S. E. Harris and T. B. Lucatorto (AIP, New York, 1984), p. 449.